SPE 56507

Effects of Wettability on Dielectric Properties of Porous Media

Buu-Long Nguyen, SPE, Johannes Bruining, SPE, Evert C. Slob, SEG

This paper was prepared for presentation at the 1999 SPE Annual Technical Conference and Exhibition held in Houston, Texas, 3–6 October 1999.

Abstract

We present in this paper the results of measurements of the complex dielectric permittivity and electric conductivity in oil-wet and water-wet porous media in a frequency range of 300kHz to 1.5GHZ. The porous media are made from unconsolidated acid-purified quartz sand which originally is water-wet. We used silylating agents to convert the same glass beads to hydrophobic oil-wetted surfaces. This avoided the effects of geometry on the dielectric permittivity that would happen if different glass grains are used.

We have made measurements in a specially designed capillary pressure cell with a built-in transmission line which goes through the porous media. The measured capillary pressure curves serve as an indication of the degree of wettability. From the scattering characteristics of the built-in transmission line, we computed the complex dielectric permittivity of the porous media as function of frequency and water saturation

We observed a significant difference in dielectric permittivity of water-wet and oil-wet porous media. At low water saturation, the dielectric permittivity of oil-wet sand is smaller than that of the water-wet one. At water saturation higher than 0.3, the dielectric permittivity of oil-wet sand becomes much larger that that of the water-wet one.

Our results with results show the same trend observed by some previous researchers, but do not agree very well with dielectric permittivity, calculated using mixing models.

This experimental study illustrates the importance of the wetting state of the porous media in determining their dielectric behavior.

Introduction

The complex permittivity, next to the electric conductivity, is one of the most useful measures for hydrocarbon exploration and shallow subsurface investigation in groundwater contamination problems. Water and oil saturation can be computed from the dielectric permittivity using dielectric mixing models.

The dielectric permittivity of any multicomponent system is generally considered to depend upon the volume fraction and dielectric permittivity of each individual component. It is commonly assumed in theoretical modeling of dielectric properties that the dielectric response of individual components do not change when the components are combined to form the total system. To the best of our knowledge, existing mixing models are based on the volume fractions and the dielectric permittivity of every component of the porous media and do not account for the effect of wettability. Because reservoir rocks and soils can be in different states of wettability, it is important to investigate and to understand the effects of wettability on dielectric properties in order to properly predict water saturation.

Different values of dielectric permittivity of water-wet and oil-wet sandstones have been observed by Poley et al. [1]. The authors concluded however that there is an average behavior of samples of different wettability. Based on experimental measurements of dielectric properties of rocks in a frequency range of 10Hz-10MHz, Garrouch and Shrama concluded that wettability has only a small influence on the dielectric permittivity of fully brine-saturated rocks. Knight and Abad (1995) measured dielectric permittivity of hydrophobic sandstones at 1Mhz and found that hydrophobic sandstones possess a lower dielectric permittivity that the hydrophilic ones, for water saturations ranged from 0 to 1.0. They also found that both the hydrophilic and hydrophobic data can be described by the complex refractive index model (CRIM) with a corrected porosity [3].

Most of modern electromagnetic tools and measuring techniques operate in the frequency range of 15Mhz to 1.1GHz. The Electromagnetic Propagation Tool, one of the more widely used dielectric tools, operates, for example, at

1.1GHz. Ground Penetrating Radar equipments operate in the frequency range of 80MHz-900MHz.

As the polarization mechanism at 10MHz to 10 GHz frequencies are of molecular and electronic kind, while polarization at lower frequencies (10Hz-10Mhz) is mainly caused by ionic double-layer polarization phenomena at the solid-fluid interface, we expect that the difference in dielectric behavior of hydrophilic and hydrophobic porous media could have another features.

In the first section of this paper, we described the experimental procedure. We further present and discuss the experimental results and results of modeling using a number of existing mixing models. Appendix A describes the measurements of capillary pressure curves. Appendix B briefly presents the procedure of analyzing the scatter function measured with the built-in Frequency Domain Reflectometry (FDR) probe.

Experimental Procedure

Measurement Principles. The main part of the experimental setup (Fig.1) is the capillary pressure cell equipped with a three-wires FDR probe that goes through the porous medium (Fig.2). The capillary pressure cell enables us to measures the whole drainage-imbibition cycle for any sample, while the FDR probe measures the dielectric response of the porous media.

The input side of the FDR probe (No.14 in Fig.2) is connected with a Network Analyzer (in Fig.1) by a standard lowless 50Ω coaxial cable. The output side of the probe is designed as a female SNC connector (No.10, Fig.2) providing possibility for attaching standard terminations (open, short and/or load) or for transmission measurements.

The transition units (No. 11, Fig.2) are designed to have the standard impedance of 50Ω to avoid additional reflections.

We measure the S_{11} scatter function at every data point on the drainage and imbibition curves. The dielectric properties of the samples at every capillary pressure/saturation data point cab then be obtained by applying a standard complex irritation The definition of the S_{11} scatter function and the principles of its measurement have been described in details in our previous work [4]. The optimization procedure and its validation has been also presented earlier [4]. For the readiness of this paper we will give a brief description of these principles in App. B.

The operating principles and measuring procedure of the capillary pressure cell is described in Appendix A.

Materials and Preparation of Experiments. The porous media are made from unconsolidated acid-purified quartz sand which originally is water-wet. The sand is fairly well-sorted with grain size varying between 80μm and 225 μm. We used silylating agents to convert the same glass beads to hydrophobic oil-wetted surfaces. This avoided the effects of geometry on the dielectric permittivity that would happen if different glass grains are used. The applied silylating procedure has been described and evaluated by Ref.5.

Capillary pressure - water saturation curves measured during the experiments serve as an indication of the extent, to which each sample had been altered from a hydrophilic to a hydrophobic state.

The porous medium is packed into the coaxial cell using a "particle distributor" [6]. The method appeared to give uniform lateral and longitudinal deposition of sand. With this technique we manage to get an average porosity of 0.420±0.005 for water-wet samples and an average porosity of 0.470±0.005 for oil-wet samples. The porosity of the porous medium is determined for every experiment. The working fluids are *n*-decane and distilled water. The capillary pressure cell filled with sand is then slowly flooded with water or with *n*-decane, depending on the experimental scenario's. The water-wet and oil-wet samples are initially saturated with water and n-decane, respectively. During the flooding the cell is put on its side and the flooding fluid flows in the cell from below and flows out on the upper side through the connectors (No. 9, Fig.2). After approx. 10 pore volumes, the flooding process is terminated and the cell is put again in horizontal position.

Validation of the Optimization Procedure. This is the first time we performed measurements with a FDR probe, in which a section with non-standard impedance is embedded between sections of standard impedance (50Ω). To validate the reliability of the optimization procedure, we have made measurements in n-butanol (ε_r • 18) and ethanol (ε_r • 25). These fluids are used as standard media because of their well-known dielectric properties. Besides their dielectric permittivities are of the same range as that of fluid-saturated porous media.

For the validating measurements, the cell is filled with subsequently with n-butanol and ethanol. The optimization procedure is then applied to find the values of the Debye's parameters (App. B) ε_s, ε_{inf} and f_{rel}.. We present the optimized parameters in Table 1 and 2 together with the parameters found in the literature [7]. The parameters show close agreement.

We simulate the scatter function with the two Debye's parameters sets. We call them *literature* and *optimized*, respectively. The simulation results are compared with the measured scatter function in Fig. 3 for a frequency range of 300kHz to 3GHz. Up to 1.5 GHz the *literature* and measured scatter functions follow each other very well. At frequencies higher than 1.5GHz, noticeable difference in amplitude and phase appear. This might be related to the non-ideal coaxial character of the built-in probe, and its length. To ensure the reliability of measurement results for the purpose of this study we will work with the frequency range 300kHz-1.5GHz.

We than calculate the complex relative dielectric permittivity of the two fluids using the Debye's equation for frequencies up to 1.5GHz. The results are compared in Fig. 4. At low frequencies, the relative errors for butanol is up to 5.4%, but at frequencies higher than approx. 200MHz, the

errors are under 3%. The errors for ethanol do not exceed 4% for the whole working frequency range. In our opinion, these errors fairly acceptable.

Results of Measurements in Water-Wet and Oil-Wet Sand Samples

Figure 5 shows the average capillary curves measured during the primary drainage of the water-wet and silylated samples. The silylated samples show a clear oil-wet behavior. This proves the reliable of the silylating procedure.

Figure 6 presents the real part of the S_{11} scatter functions measured at water saturation S_w= 0.43 in water-wet and oil-wet samples. The clear difference in phase as well as in amplitude suggests that the dielectric properties of the samples should be different too.

In Fig.7 we show the real part of the complex relative dielectric permittivity (ε') of the water-wet and oil-wet samples at 300kHz, 750MHz and 1.1 GHz. As the real part of the dielectric permittivity decreases very slightly in the working frequencies, we do not show their frequency dependence on a separate graph.

We observe differences not only in the value of the dielectric permittivity but also in the form of the $\varepsilon'(S_w)$ curve. The convex side of the $\varepsilon'(S_w)$ curve for water-wet samples is downward, while it is upward for the oil-wet samples.

At low water saturation (S_w<0.25) and low oil saturation (S_w>0.80), hence when the fluid saturation approaches the residual values, the dielectric permittivity of the oil-wet samples is smaller than that of the water-wet ones. The low values of the dielectric permittivity of the oil-wet samples might be caused by the presence of a insulating oil film along the surface of the glass grains. However to understand the mechanism that leads to higher values of dielectric permittivity of oil-wet samples, compared with those of the water-wet ones, we need to know more about the fluid distribution inside the samples during the saturation process.

It is interesting to note that previous researchers had observed the same trend of differences in dielectric permittivity of oil-wet and water-wet porous media [1]. The oil-wet samples had been also made from water-wet sandstone by a silane treatment. They attempted, however to draw an average line through the data, ignoring meanwhile the difference. For comparison purposes, we have reconstructed their experimental data in Fig. 8a. The original graphic material can be found in Ref.1 (Fig.20). The oil-wet data cover only a limited saturation range. However, we still can observe that the oil-wet dielectric permittivity is lower that the water-wet one at low saturation. The difference in the curve form is also similar which what we observed in our experimental results.

Modeling with Mixing Models

In Fig.8 we also show the real parts of the complex relative dielectric permittivity calculated with the Bruggelman-Hanai-Sen formula (Eq.1, App.C) and the CRIM (Eq.3, App.C) for our samples. Background information over these models is given in App. C.

The oil-wet dielectric permittivity modeled with the OW-I model (see App.C for explanation) and the CRIM is also smaller than that of the water-wet samples at saturation below approximately 0.50. However, we do not recognize the curve form, characteristic for our oil-wet data. It is worth noting that the simulation results obtained with the CRIM do not show the same trend presented in Ref.3. Difference in working frequency might play a role.

The values oil-wet dielectric permittivity modeled with the OW-I model (see App.C for explanation) are far below those of the water-wet samples. The assumption of zero-water-phase percolation threshold in this approach is, however, questionable.

Conclusions

We introduce a new experimental setup for simultaneous measurement of capillary pressure/saturation curves and dielectric response of fluid-saturated porous media.

We obtained different values of complex dielectric permittivity and electric conductivity at the same water saturation in porous media of different wettability.

At low water and oil saturations, the dielectric permittivity of oil-wet media are lower than those of the water-wet ones. This might be caused by the presence of a insulating oil film along the surface of the sand grains.

When the water saturation is known, data obtained with electromagnetic tools can be used as an indication of reservoir wettability.

Our future work is focused on the effects of fluid distribution, which is different in water-wet and oil-wet systems at the same saturation, on the dielectric properties of the systems. The effects of other factors, e.g. spreading coefficient, the present of finite clusters of both fluids, are also being investigated.

References

1. Poley, J.Ph., Noteboom, J.J. and de Waal, P.J.: " Use of VHF Dielectric Measurements for Borehole Formation Analysis" - *The Log Anal.*, Vol. XIX, No. 3, 1978, 8-30.
2. Garrouch, A.A. and Sharma, M.M.: "The Influence of Clay Content, Salinity, Stress, and Wettability on the Dielectric Properties of Brine-Saturated Rocks" - *Geophysics*, Vol. 59, No.6, 1994, 909-917.
3. Knight, R. and Abad, A.: "Rock/Water Interaction in Dielectric Properties: Experiments with Hydrophobic Sandstones" - *Geophysics*, Vol. 60, No.2, 1995, 431-436.
4. Nguyen, B.L., Geels. A.M., Bruining J. and Slob, E.C.: "Calibration Measurements of Dielectric Properties of Porous Media" - *SPE 38715, Proc.*of the 1997 SPE ATCE, San Antonio, Vol. Ω, 13-21.
5. Olsen, D.K. and Crocker, M.E.: "Evaluation of Artificial Wetted Surface for Use in Laboratory Steamflood Experiments" - *Proc. of* the *Conference* "Heavy Crude and Tar Sand - Hydrocarbons for the 21st Century, 373-378.
6. Wygal, R.J.: "Construction of Models that Simulate Oil

Reservoirs", *Society of Petroleum Engineers Journal*, 281-286, December 1963.
7. Gemert van, M.J.C.: "High-Frequency Time-Domain Methods in Dielectric Spectroscopy" - *Philips Research Rep.*,1973, 28, 530-572.
8. Lingen, van P.P., J. Bruining and C.P.J.W. van Kruijsdijk: "Capillary Entrapment due to Small-Scale Wettability Heterogeneities" - *SPE 30782, Proc.*of the 1995 SPE ATCE, Dallas, Vol. Σ 829-843
9. Press, W.H., Teukolsky, S.A., Vetterling, W.T. and Flannery, B.P.: *Numerical Resipes in C: the Art of Scientific Computing*, 2d Edition, Cambridge U. Press (1992).
10. Hasted, J.B. - *Aqueous Dielectric*. London, Chapman & Hall, 1973.
11. Beek, van L.K.H.: "Dielectric Behavior of Heterogeneous Syatems" - in *Progress in Dielectrics*, Vol.7, J. Birks, Ed. Cleveland, OH: CRC Press, 1965, 69-114.
12. Hanai, T.: "Dielectric theory on the Interfacial Polarization for Two-Phase Mixtures" - *Bull. Intl. Chem. Res.*, Kyoto U., 1961, Vol. 39, 341-368.
13. Wobschall, D.: " A Theory of the Complex Dielectric Permittivity of Soil Containing Water: The Semidisperse Model" - *IEEE Trans.on Geosc. Elec.*, 1977, Vol. GE-15, No.1, 49-58.
14. Sen, P.N., C. Scala and M.H. Cohen: "A Self-Similar Model for Sedimentary Rocks with Application to the Dielectric Constant of Fused Glass Beads", *Geophysics*, 46(5), 781-795, May 1981.
15. Feng Sh. And Sen, P.N.: "Geometrical Model of Conductive and Dielectric Properties of Partially Saturated Rocks" - *J. Appl. Phys.*, 1985, 58(8), 3236-3243.

Appendix A. Modeling the S_{11} Scatter Function and the Optimization Procedure

In our previous work [4], we have the recursive expression for the multiple reflection coefficient at the n^{th} interface in a n-sectional coaxial transmission line. The general form is given by:

$$R_n = \frac{r_n + R_{n+1}\exp(-2\gamma_{n+1}l_{n+1})}{r_n R_{n+1}\exp(-2\gamma_{n+1}l_{n+1})+1} \quad \text{..... (B-1)}$$

where $l_{n+1}=z_{n+1}-z_n$ is the length of the $(n+1)^{th}$ part, and

$$r_n = \frac{Z_{n+1}-Z_n}{Z_{n+1}+Z_n} \quad \text{..... (B-2)}$$

is the reflection coefficient due to change in impedance at the n^{th} interface.

If the transmission line is terminated with a load impedance, $R_{n+1} = 0$. When it is short-circuited, $R_{n+1} = -1$ and R_{n+1} will be unity if the line is open-ended.

The FDR probe built in the capillary pressure cell is designed with a female standard SNC connector. That allows for connecting of standard termination. For each saturation point, measurements have been made with open, short and load termination connected.

As we proved in [4] the S_{11} scatter function measured with the network analyzer equals the multiple reflection coefficient at the interface between the connecting cable and the probe. The procedure is as follows

- we measure the S_{11} scatter function of every sample with unknown dielectric properties.
- we use our reflection model to calculate the theoretically expected S_{11} scatter function. For this purpose we have to suggest some begin values for the Debye's parameters, ε_s ε_∞, f_{rel} (see explanation below).
- we apply then a standard complex iteration technique [9] to optimize the suggested Debye's parameters in such a way that the difference between the measured and theoretically calculated S_{11} scatter function will be minimum.
- the relative complex dielectric permittivity can then be calculated with the Debye's equation (Eq.B3).

We assume that the frequency dependence of the complex dielectric permittivity $\varepsilon^*(f)$ of sand saturated with water and oil can be described by the Debye's equation

$$\varepsilon^*(f) = \left(\varepsilon_\infty + \frac{\varepsilon_s - \varepsilon_\infty}{1+(if/f_{rel})}\right) - \frac{i\sigma_{dc}}{2\pi f\varepsilon_0} \quad \text{..... (B-1)}$$

where ε_s, ε_∞ are static and infinite (apparent) dielectric permittivities, respectively; f_{rel} is the relaxation frequency and ε_o is the vacuum permittivity.

Appendix B. Notes on Mixing Models

In this Appendix, we give a brief review of two mixing models which have the ability to differently model dielectric permittivity of oil- and water-wet systems.

A mixing model that is often mentioned in geophysical literature is the Bruggelman-Hanai-Sen formula

$$\frac{\varepsilon_h^* - \varepsilon_m^*}{\varepsilon_h^* - \varepsilon_i^*}\left(\frac{\varepsilon_i^*}{\varepsilon_m^*}\right)^{1/3} = f_{vi} \quad \text{..... (1)}$$

where ε_m^*, ε_h^* and ε_i^* are the dielectric permittivity of the composite, the host medium and the inclusion, respectively; f_{vi} is the volume fraction of the inclusion. This well-known Bruggelman [10,11] formula arrived at by the method of iterations and generalized for complex dielectric permittivities by Hanai [12]. According to Ref.13 this Bruggelman-Hanai formula is successful in describing the dielectric behavior of soils containing moisture at high frequencies (1MHz-1GHz). Sen et al [14] used this model to develop a self-similar model for sedimentary rocks.

Feng and Sen [15] developed this model further and show theoretically how the model can be used to calculate dielectric permittivity of water- and oil-wet porous media. For water-wet system, the oil is considered to be dispersed in the water phase. The dielectric permittivity of the fluid phase is then calculated with Eq.1. Subsequently the fluid phase is considered to be dispersed in the matrix of solid phase.

For oil-wet systems they distinguish two cases: a) case where the oil phase is continuous and the water case forms

droplets, b) case where the water phase is continuos and the oil phase forms coating of matrix grains. In case a) the role of oil and water is interchanged in the formalism just mentioned above. In the main text of this paper, we refer to this approach as model OW-I. For case b) Ref.15 suggests first to calculate the dielectric permittivity of the coated grains by:

$$\varepsilon_{m,eff} = \varepsilon_o \left(\frac{\varepsilon_m + 2\varepsilon_o + 2\xi(\varepsilon_m - \varepsilon_o)}{\varepsilon_m + 2\varepsilon_o - 2\xi(\varepsilon_m - \varepsilon_o)} \right) \quad \ldots\ldots\ldots\ldots\ldots (2)$$

in which

$$\xi = (1-\phi)[(1-\phi+\phi(1-S_w)]$$

ε_m and ε_o are the dielectric permittivity of matrix and oil, respectively; ϕ is the porosity and S_w is the saturation. Then the dielectric permittivity of the rock with zero-water-phase percolation threshold is simulated by the two-phase self-similar model (Eq.1). In the main text of this paper, we refer to this approach as model OW-II.

Another mixing model that seems to be able to account for wettability is the complex refractive index model (CRIM).

$$\sqrt{\varepsilon_m^{\alpha}} = \sum_{i=1}^{n} f_{vi} \sqrt{\varepsilon_i} \quad \ldots\ldots\ldots\ldots\ldots\ldots\ldots\ldots\ldots (3)$$

where ε_m and ε_i are dielectric permittivities of the n-component material and of the i^{th} component, respectively; f_{vi} is the volume fraction of the i^{th} component. When dealing with water-wet samples saturated with air and water, Ref.3 considers the matrix as wetted rock, which is the dry rock plus the surface water, coating the solid at saturation smaller than some critical water saturation S_w^o. The porosity is than corrected by:

$$\phi_c = \phi - S_w^o \phi \quad \ldots\ldots\ldots\ldots\ldots\ldots\ldots\ldots\ldots\ldots\ldots\ldots (4)$$

In case of hydrophobic rock, Ref.3 considers the matrix as dry rock. The authors show that the CRIM justified in such a way described very well the behavior of both hydrophilic and hydrophobic samples at least at 1MHz, which is the working frequency during the experiments. In all cases, the dielectric permittivity of hydrophobic samples are smaller that that of the hydrophilic ones.

In this paper we defined the corrected porosity of the water-wet and oil-wet samples as follows:

$$\phi_c = \phi - S_{rwt} \phi \quad \ldots\ldots\ldots\ldots\ldots\ldots\ldots\ldots\ldots\ldots\ldots\ldots (5)$$

where S_{rwt} is the residual saturation of the wetting phase

Table 1 Comparison between the Cole-Cole parameters for n-butanol at 24^{0}C

Source	ε_s	ε_∞	f_{rel} (Hz)
van Gemert [7]	17.7	3.33	0.274e9
experiment	16.76	3.18	0.288e9

Table 2 Comparison between the Cole-Cole parameters for ethanol at 24^{0}C

Source	ε_s	ε_∞	f_{rel} (Hz)
van Gemert [7]	24.75	4.55	0.902e9
experiment	24.07	5.64	0.838E9

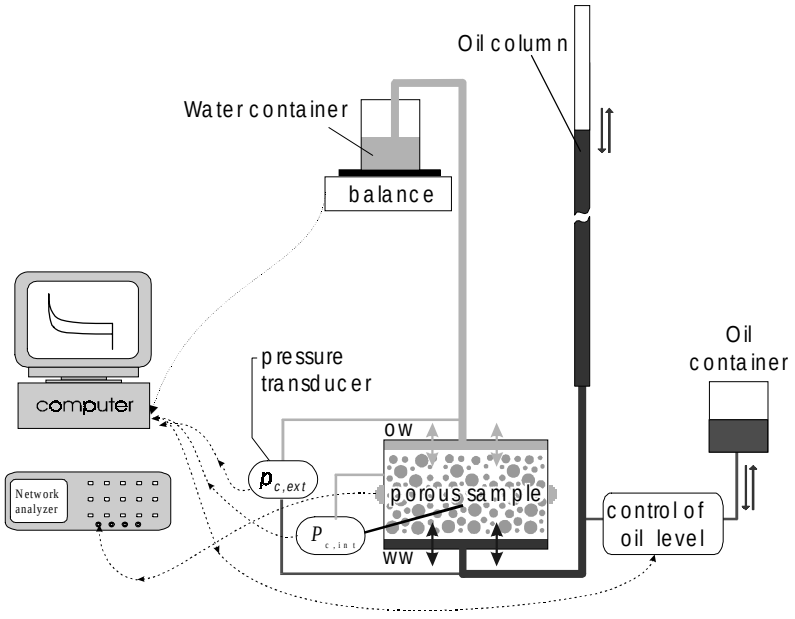

Figure 1 - Schematic presentation of the experimental setup

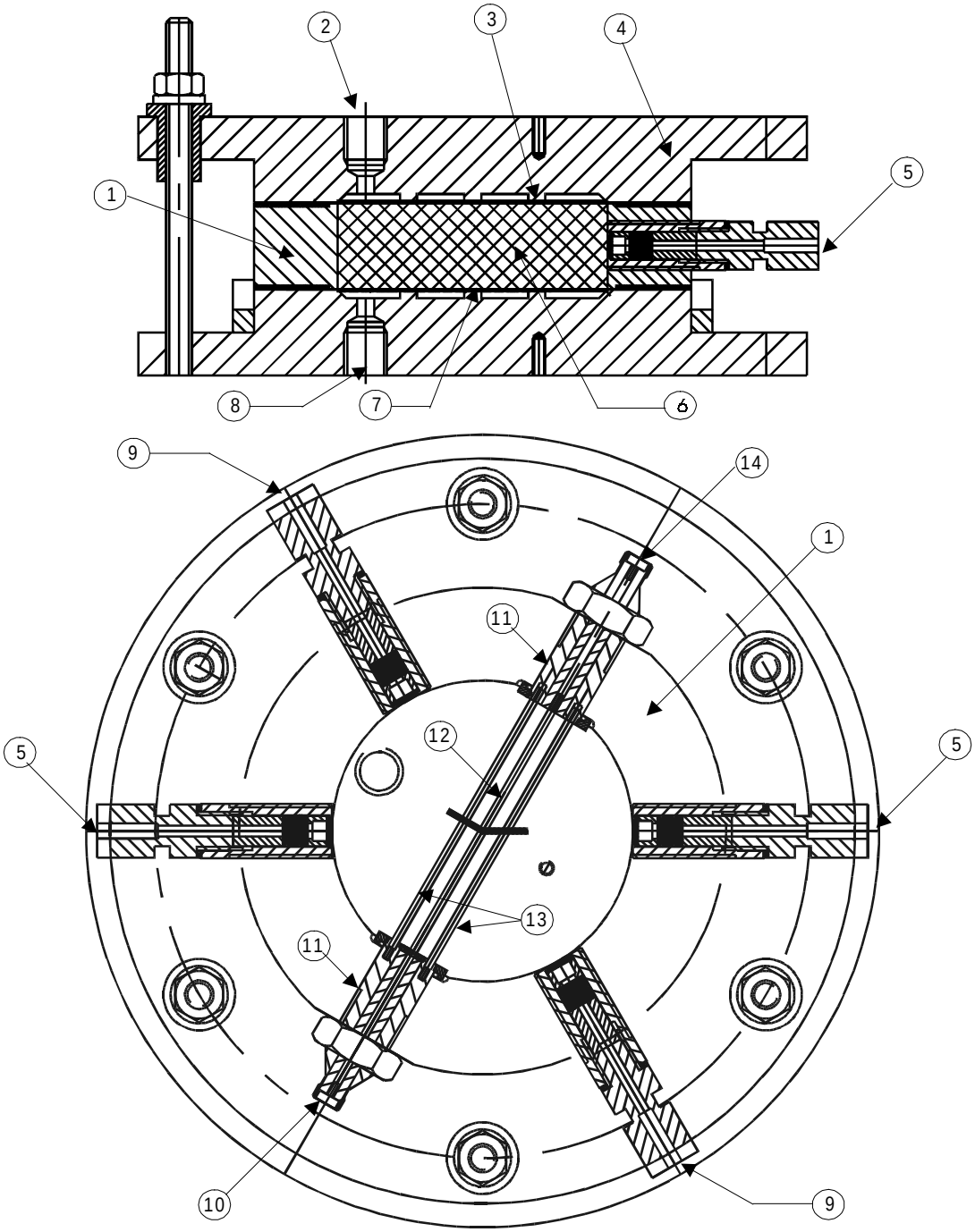

Figure 2 - Capillary pressure cell with a built-in transmission line (FDR probe): 1. The cell; 2. Oil inlet; 3. Oil-wet filter; 4.Cover; 5. Pressure taps (connected with DPT); 6. Porous medium; 7. Water-wet filter; 8. Water inlet; 9. Channel for fluid flooding; 10. Connector at the input side of the FDR probe; 11. Transition units; 12. Inner conductor; 13. Outer conductor.

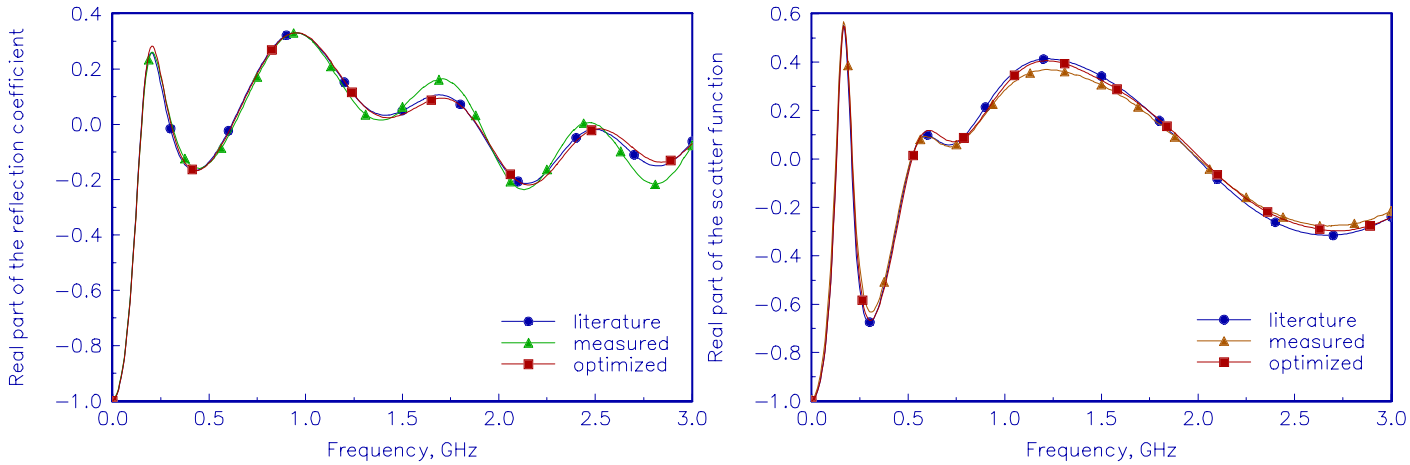

Figure 3 - Simulated, measured and optimized S_{11} scatter function for n-butanol (left) and ethanol (right)

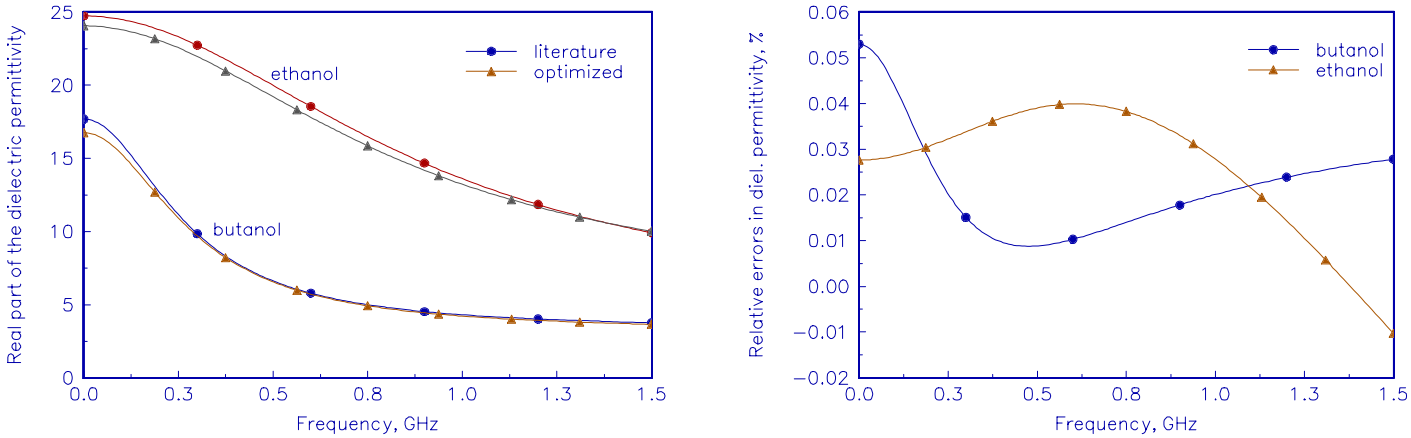

Figure 4 - Dielectric permittivity simulated with literature and experimentally obtained values of the Debye's parameters for butanol and ethanol (left) and the relative errors between the literature and experimental values (right)

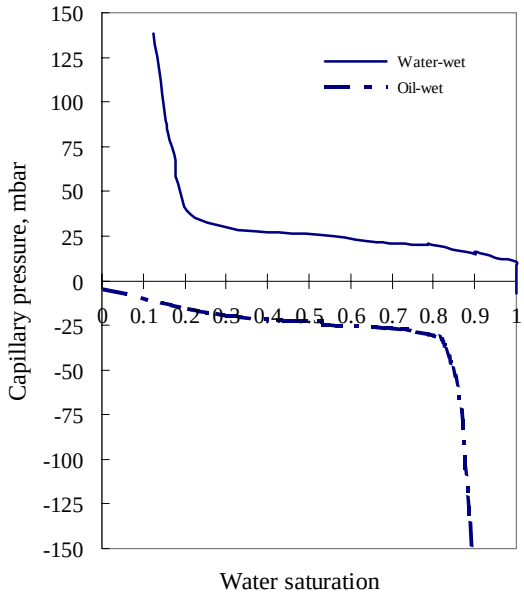

Firgure 5 (left) - Capillary pressure curves measured in water-wet and silylated (oil-wet) samples

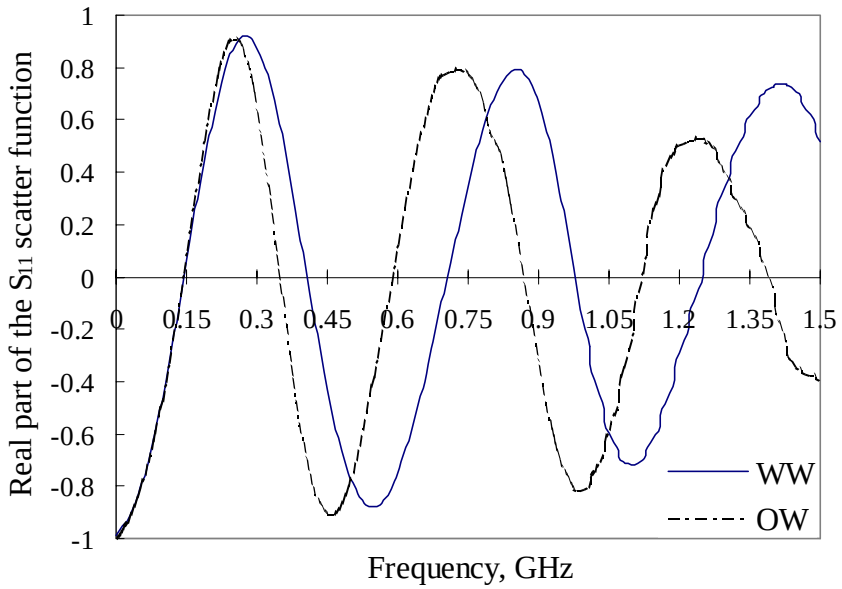

Figure 6. Scatter functions measured in water- and oil-wet samples at Sw=0.43

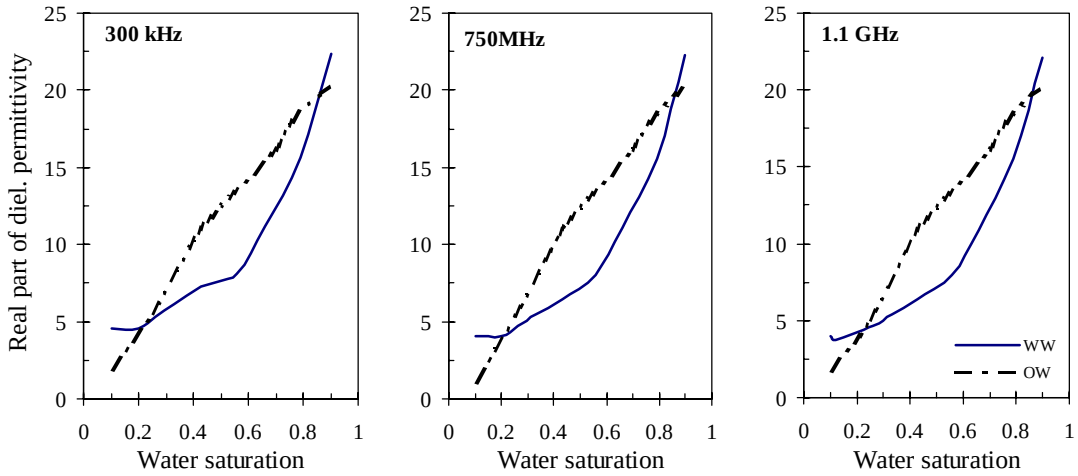

Figure 7 - Real part of the dielectric permittivity obtained from S_{11} measurements in water- and oil-wet samples at different frequencies

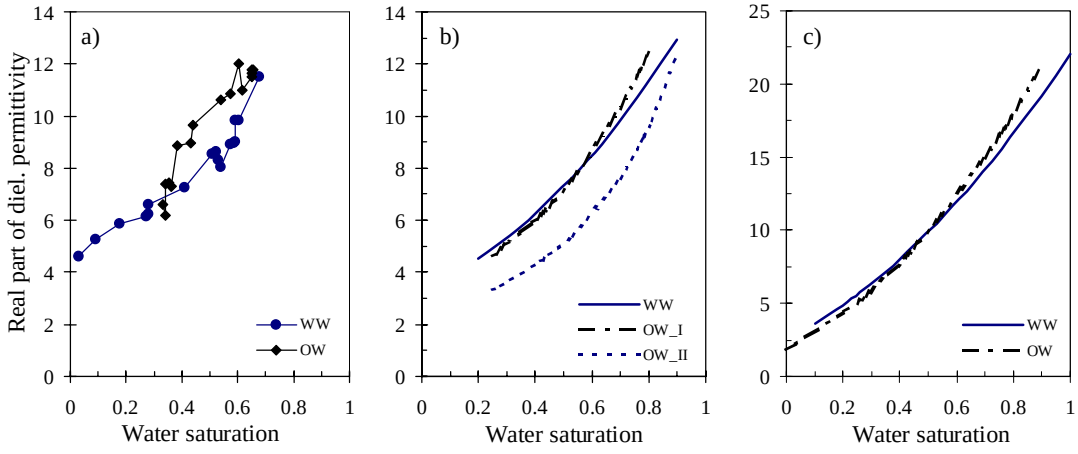

Figure 8 - a) Dielectric permittivity of water- and oil-wet sample at 250MHz (reconstructed from Fig.20, Ref.1); b). Modeled with the BHS model for our samples at f=1,1GHz; c). modeled with the CRIM at 1.1GHz